Mechanics & Industry 15, 541–549 (2014)

DOI: 10.1051/meca/2014060
www.mechanics-industry.org

Mechanics & Industry

Modal parameters of the human hand-arm using finite element and operational modal analysis

S. Adewusi, M. Thomas[a], V.H. Vu and W. Li

Research Laboratory in Machinery, Process and Structural Dynamics (DYNAMO), Mechanical Engineering Department, École de Technologie Superieure 1100 Notre-Dame Street West, Montreal, Quebec, H3C 1K3, Canada

Received 17 June 2013, Accepted 15 May 2014

Abstract – This study presents a finite element (FE) model of the human hand-arm system to derive natural frequencies and mode shapes. The FE model is calibrated by considering modal parameters obtained from experimental vibration analyzed by using operational modal analysis (OMA) and transmissibility. Modal and harmonic analyses of the FE model are performed for two boundary conditions. The first one considers fixed shoulder condition while the second one introduces the trunk in order to permit motion of the shoulder. The results show that the natural frequencies of the second model that permits shoulder motion are comparable with those determined from measurements. Especially, the natural frequency about 12 Hz, which is corresponding to the frequency of maximum weight in ISO-5349-1 (2001), is not present in the model with fixed shoulder condition, while it appears in the second model. The results of the present study suggest that improved finite element models of the human hand-arm system may reveal hand-arm injury mechanism, the understanding of which may assist in deriving appropriate frequency weightings for the assessment of different components of the hand-arm vibration syndrome.

Key words: Hand-arm system / finite element / vibration measurements / ISO 5349-1

1 Introduction

Several epidemiological studies on workers exposed to prolonged hand-transmitted vibrations (HTV) have revealed various injurious effects like vascular, sensorineural and musculoskeletal disorders, generally referred to as the hand-arm vibration syndrome (HAVS) [1]. This has inspired research efforts about the dynamic characteristics of the human hand-arm system exposed to vibration (biodynamic responses) [2] and assessment of potential injury associated with prolonged exposure to HTV [3]. Although these research efforts have enhanced understanding of the health problems associated with occupational exposure to HTV and have led to several International Standards on how to measure, assess and mitigate the effects of HTV, the hand-arm injury mechanism due to vibrations is not yet fully understood. Furthermore, there are considerable discrepancies between injury assessments based on the current ISO 5349-1 [4] guidelines and epidemiological studies [1,3,5]. The development of a reliable hand-arm model may reduce variations in the reported biodynamic properties of the human hand-arm system and may enhance understanding of hand-arm injury mechanism. Although the human hand-arm is a non-uniform, nonlinear, anisotropic and composite system, lumped-parameter models and continuous model based on beam theory have been developed to characterize biodynamic responses and energy absorption characteristics of the hand-arm substructures [6]. The authors of the studies [6] admitted that the lumped models did not represent the continuous fingers-hand-arm system and may not accurately predict location-specific responses. A recent study [7] presented biomechanical models of the hand-arm system, derived from both the driving-point mechanical impedance (DPMI) and transmissibility responses with the consideration of hand-arm arm postures and anatomical structure. However, the masses of the bones and muscles/tissues of the forearm and upper-arm of these models were lumped together to form rigid members. A very recent preliminary study has suggested that finite element (FE) models may provide the vital information needed to understand injury mechanism of the human hand-arm exposed to vibration, and reliable identification of hand-arm resonant frequencies [8]. The preliminary study however assumed a fixed shoulder condition with bones connected at joints with ligaments. These assumed conditions may not represent the actual condi-

[a] Corresponding author: marc.thomas@etsmtl.ca

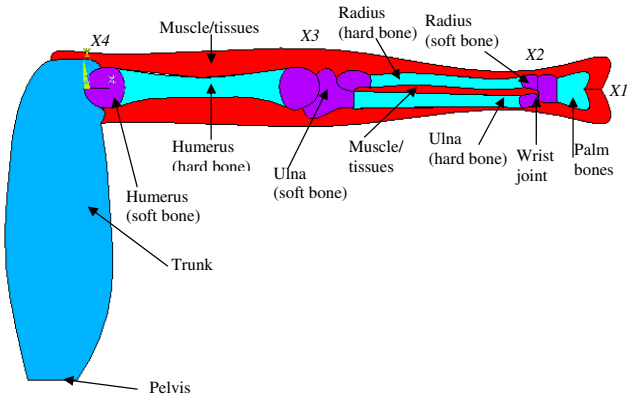

Fig. 1. Components and substructures of the human hand-arm FE model.

Table 1. Dimensions of the hand-arm of six subjects.

Hand-arm length and projected dimensions on a plane			
Parameters	Ranges	Mean	STD
Age (years)	26–53	36.5	11.33
Height (cm)	171–180	174.0	0.02
Weight (kg)	61–86	72.2	9.87
BMI	20.4–28.7	23.8	3.13
Hand length (cm)	17–20.5	18.4	1.20
Hand width at thumb (cm)	9.5–12.0	10.9	0.86
Hand width at metacarpal (cm)	7.0–8.5	7.5	0.63
Hand thickness (cm)	2.0–3.7	2.9	0.55
Wrist width (cm)	5.1–5.9	5.5	1.04
Forearm width (cm)	8.0–10.0	8.9	2.53
Elbow width (cm)	7.8–9.7	8.4	2.22
Forearm length (cm)	24.0–28.5	26.0	1.58
Upper arm width (cm)	8.9–10.5	9.0	3.13
Upper arm length (cm)	23.0–32.0	28.5	2.35

tions of the hand-arm of the operators of hand-held power tools.

The hypothesis of the present study is that finite element model of the human hand-arm system will yield reliable identification of the resonant frequencies and mode shapes of the hand-arm system. This study presents finite element (FE) model of the hand-arm system to determine the natural frequencies and mode shapes of different substructures of the human hand-arm. Two boundary conditions are imposed on the FE models namely: (1) the entire trunk is fixed to produce fixed shoulder condition, and (2) the trunk is fixed at the pelvis to permit motion of the shoulder. The natural frequencies of the FE model are also estimated from responses computed at different locations due to a simulated harmonic excitation considering damping. In order to calibrate these models and determine which model is more representative of the human hand-arm, the natural frequencies of the FE models are compared with those derived from measured transmissibility and those obtained from operational modal analysis (OMA). The autoregressive moving average (ARMA) technique as proposed by Vu et al. [9] has been applied to experimental acceleration measurements using output only.

2 Methods

2.1 Finite element (FE) model

Two-dimensional (2D) FE model of the human hand-arm, which consists of the palm, forearm, upper-arm and the joints, is presented in Figure 1. The fingers are not considered since a few studies [10] have presented the 2D FE model of the fingertip, which may be considered as a representative model of the fingers. Figure 1 presents the hand-arm model in the extended arm posture consisting of the trunk, humerus bone, radius and ulna bones, bones of the palm (carpals bones lumped together), and muscles/tissues.

The humerus, radius and ulna bones consist of the cortical (hard) bone around the mid-span and trabecular (soft) bones at the ends. The bones are assumed to be in contact at joints and then held together by muscles/tissues. The mean anthropometric dimensions (Tab. 1) of the hand-arm of 6 subjects who participated in the laboratory measurements of transmissibility responses of the human hand-arm system exposed to z_h-axis vibration [11] and the reported bone dimensions were used to develop the FE model in ANSYS using the SI system of units. $X1$, $X2$, $X3$ and $X4$ represent in Figure 1, locations near the palm, wrist, elbow and shoulder, respectively, where responses of the model are observed. Most of the laboratory studies on effects of hand-arm posture on the biodynamic responses considered either the bent-arm (90° elbow angle) or the extended arm (180° elbow angle) postures [2,11]. Furthermore, the posture (about 155° elbow angle with about 30° abduction angle) of the operator of road breakers is close to the extended arm posture (180° elbow angle). Although the posture assumed by an operator of the hand-held power tool depends on the type of tool and the kind of the operation being performed, the extended hand-arm posture, as shown in Figure 1, is modeled in this study for simplicity and in order to compare the FE model results with available experimental data.

2.1.1 FE model with fixed shoulder

The majority of the reported lumped-parameter models assumed a fixed shoulder condition even though some studies have reported substantial vibration at the shoulder [11,12]; motion of the trunk and the head was also reported in extended arm posture [13]. The fixed shoulder condition of the first model is achieved in this study by applying fixed boundary condition (zero displacement) to the entire trunk so that is does not move.

2.1.2 FE model with motion of the shoulder

The second model with the relaxation of the fixed shoulder condition to permit the motion of the shoulder is obtained by changing the boundary condition imposed

Table 2. Mechanical properties of the components of the human hand-arm system.

	Cortical bone	Trabecular bone	Muscles/tissues
Young modulus (MPa)	7230−17000	43.6−1060	345−888
Poisson ratio	0.3	0.3	0.3
Density (kg.m^{-3})	1.5−2.0 × 10^3	1.0−7.0 × 10^3	0.75−1.2 × 10^3

on the model in Figure 1. Fixed boundary condition is applied at the pelvis only to allow for motion of the trunk and hence the shoulder. All the components of the human trunk (spines, scapular, abdomen, etc.) are lumped together as shown in Figure 1 to simplify the model and since this study focuses on the hand-arm.

2.1.3 Modal and harmonic analyses of FE models

The ranges of the reported values for the mechanical properties of cortical and trabecular bones, and muscles/tissues [14–16], as summarized in Table 2, are used for the FE simulations using ANSYS. Although the reported properties of bones are for the femur bone, the properties of the hand-arm bones are assumed to be similar to those of the femur. Plane182 element type is used for the tissues/muscles since this element type has plasticity, hyper-elasticity, stress stiffening, large deflection, and large strain capabilities. Other components are represented with Plane183 element type, which is good for modeling irregular shapes. The FE analysis is performed in two steps using ANSYS. The first step consists of harmonic analysis of the model that permits motion of the shoulder when an excitation force of 50 N in the z_h-axis direction is applied at the palm side. A force of 50 N was applied because the transmissibility responses reported in [11] correspond to 50 N push and 30 N grip forces. It should be noted that the x- and y-axis in ANSYS correspond to the z_h- and y_h-axis, respectively, of the hand-arm coordinate system defined in ISO 5349-1 [4].

Rayleigh damping coefficients are estimated from the resonant frequencies and damping ratios obtained from measured transmissibility responses using half-power concept and those obtained from operational modal analysis (OMA) of the measured acceleration time signals. During the simulations, the mechanical properties of the trunk and muscles/tissues are varied while the lower values of Young modulus and higher values of density of the bones were maintained until some of the resonant frequencies of the model are comparable with those obtained from OMA using autoregressive moving average (ARMA) technique. The properties of the trunk and muscles are varied since mechanical properties of the trunk are not known and the properties of the muscles/tissues depend on hand forces and hand-arm posture. The harmonic responses are computed at four different locations marked $X1-X4$ on Figure 1. These responses correspond to deformations, in the frequency domain, around the palm side ($X1$), the wrist ($X2$), the elbow ($X3$) and the shoulder ($X4$). The mechanical properties obtained are used for all other analyses with different boundary conditions. The second step is the modal analysis to determine the natural frequencies and mode shapes of the model for fixed shoulder condition and the condition that permits motion of the shoulder. The natural frequencies of the two models are compared to study the effect of boundary condition of the shoulder on the natural frequencies of the hand-arm system in the extended arm posture.

2.2 Estimation of resonant frequencies from measured transmissibility responses

Laboratory experiments have been performed to measure the transmissibility responses of the human hand-arm of six male subjects in the bent-arm and extended arm postures at the wrist, elbow and shoulder, as shown in Figure 2. An instrumented handle of diameter 40 mm with force sensors and accelerometers to measure hand forces and input excitation is attached to an electrodynamic shaker. A broadband random excitation in the 2.5−2500 Hz frequency range with rms acceleration value of 5.25 m.s^{-2} was used to excite the handle in the z_h-axis while six male subjects gripped the handle in turn with 30 N grip and 50 N push forces. The vibration transmitted to different locations on the hand-arm was measured using tri-axial PCB accelerometers attached to Velcro strips, which were tightly fastened near the joints so as to minimize the contributions due to skin artifacts. Accelerations along the y_h- and z_h-axes were measured at locations. A 12-channel 01dB Stell data acquisition system and dBRTA/dBFA32 data analysis software by 01dB Metravib were used. The sampling frequency was 6400 Hz. The coherence of the measurements was also monitored during the experiments to ensure reliability of the measured data. Each measurement was repeated three times. Detailed results were published in [11]. In the present study, the measured acceleration time signals are analyzed by OMA analysis, as described in Section 2.3. Furthermore, the transmissibility responses are re-analyzed for each subject to derive the resonant frequencies of each subject. In the previous study [11], resonant frequencies were derived from the mean transmissibility responses of the six subjects.

2.3 Estimation of modal parameters by using operational modal analysis (OMA)

The technique of operational modal analysis (OMA) by using the auto-regressive moving average (ARMA) technique and developed by Vu et al. [9] was used to estimate the natural frequencies and damping ratios of

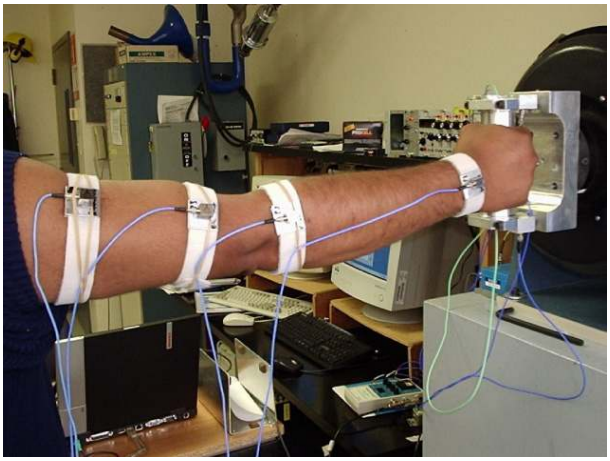

Fig. 2. Experimental set-up showing the extended arm posture.

the hand-arm system using experimentally measured acceleration time signals, as described in Section 2.2. The acceleration time signals in the y_h- and z_h-axis at different locations (wrist, elbow and shoulder) in the experimental study on transmissibility of an extended arm shown in Figure 2 are used as inputs to the Matlab code for the OMA using ARMA developed in [9]. Although the ARMA method was developed for situations where it is difficult or impossible to measure the input, it may also be used on laboratory measurements for improved identification of modal parameters of the human hand-arm. The ARMA method has been shown to give reliable estimates of modal parameters [9]. The concept of ARMA is briefly outlined in this section. If the time signals of a dynamic system are simultaneously measured at different locations using d channels with a sampling time T_s, then a multivariate ARMA model of order p and dimension d to estimate the time signals may be developed such that:

$$\{y(t)\}_{d\times 1} = [\Phi]_{d\times dp}\{\varphi(t)\}_{dp\times 1} + \{e(t)\}_{d\times 1} \quad (1)$$

where $\{y(t)\}_{d\times 1}$ is the output vector,

$$[\Phi]_{d\times dp} = \left[-[a_1] \;\; -[a_2] \ldots -[a_i] \ldots -[a_p] \;\right]$$

is the matrix of the model parameters of size $d \times dp$,

$$[\varphi]_{dp\times 1} = \left[y(t-1);\; y(t-2); \ldots; y(t-p)\right]$$

is the regressor of size $dp\times 1$, and $\{e(t)\}_{d\times 1}$ is the residual.

For N consecutive outputs of the responses from $\{y(t)\}$ to $\{y(t+N-1)\}$, the model parameters can be estimated using the least squares with QR factorization method [27]. The model is then converted to the state-space form for frequency and damping calculations, the state matrix is given as:

$$A|_{dp\times dp} = \begin{bmatrix} -a_1 & -a_2 & -a_3 & \ldots & -a_p \\ I & 0 & 0 & \ldots & 0 \\ 0 & I & 0 & \ldots & 0 \\ \ldots & \ldots & \ldots & \ldots & \ldots \\ 0 & 0 & 0 & I & 0 \end{bmatrix} \quad (2)$$

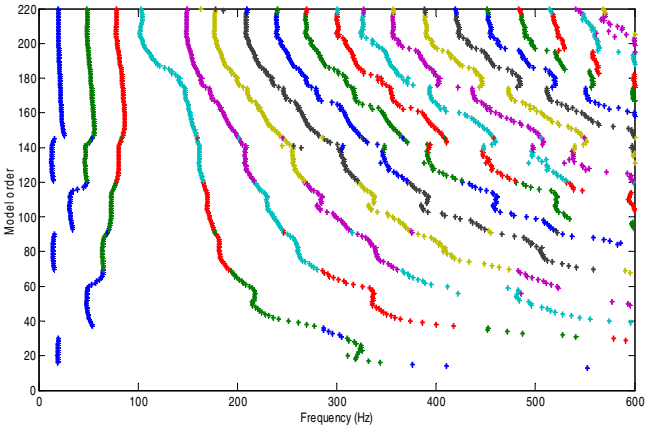

Fig. 3. Frequency stability diagram from OMA analysis.

The eigenvalue problem is then solved to determine the eigenvalues λ_i, circular frequencies ω_i, resonance frequencies f_i and the damping ratios ξ_i of the dynamic system such that:

$$[V\;\lambda] = eig(A); \quad (3)$$

$$\omega_i = \sqrt{\mathrm{Re}^2(\lambda_i) + \mathrm{Im}^2(\lambda_i)}; \quad f_i = \frac{\omega_i}{2\pi}; \quad (4)$$

$$\xi_i = -\frac{\mathrm{Re}(\lambda_i)}{\omega_i} \quad (5)$$

Figure 3 shows an example of the frequency stability diagram from which resonant frequencies are identified.

The OMA-ARMA matlab code is interactive and it permits users to specify the maximum frequency of interest and identify the best order p of the model. A maximum frequency of 600 Hz and a p of 220 were used for the analysis. The natural frequencies and damping ratios for each of the six subjects were obtained from the frequency and damping stability diagrams; the mean of these values is then calculated. We must notice that the human cannot be considered as a stationary system and that the natural frequencies may vary in time. Some of the resonant frequencies and damping ratios are used to estimate the Rayleigh damping coefficients, which are used for the harmonic analysis of the model in ANSYS. Resonant frequencies are then estimated from the FE harmonic responses of the models at the palm, wrist, elbow and shoulder.

3 Results and discussion

3.1 Natural frequencies and mode shapes of the hand-arm system

The first twenty natural frequencies of the FE model for the two boundary conditions are presented in Table 3 with remarks about which substructure has maximum deformation, as observed from the animation of the mode shapes in ANSYS.

The first twenty natural frequencies are considered to focus on 0−500 Hz frequency range. Figure 4 presents the first eight mode shapes of the model that permits the motion of the shoulder.

Table 3. Natural frequencies of the hand-arm models with fixed shoulder and moving shoulder.

	Model with fixed shoulder		Model that permits shoulder motion	
Mode #	Freq. (Hz)	Remarks (highest at)	Freq. (Hz)	Remarks (highest at)
1	8.2	Rigid rotation	5.3	Rigid rotation about the shoulder
2	39.0	Elbow	13.4	All parts (z_h-axis)
3	111.3	Palm	34.7	Elbow
4	131.4	All parts (z_h-axis)	96.2	All parts
5	190.2	All parts	107.5	Palm
6	329.4	All parts	123.3	Palm and wrist
7	342.9	All joints	184.1	All parts
8	411.4	Wrist & palm	191.2	All parts (z_h-axis)
9	459.5	Wrist & elbow (z_h-axis)	251.1	All joints
10	576.9	All parts	304.5	Shoulder and elbow
11	642.5	Palm muscle	381.9	All parts
12	700.7	Forearm & palm	385.0	Palm
13	710.4	Palm	402.4	Wrist and palm
14	769.7	Elbow	456.2	Wrist and palm (z_h-axis)
15	815.4	Elbow and palm (y_h-axis)	466.9	Elbow & Palm
16	844.2	Palm (mostly muscles)	549.1	All joints
17	846.4	Upper-arm	553.4	All joints and palm muscles
18	904.6	Palm, wrist and elbow muscles	609.8	Elbow and palm muscles
19	932.3	Upper-arm muscles	616.5	Trunk
20	953.7	Shoulder and elbow muscles	642.6	Palm muscles

Table 3 shows substantial differences in the natural frequencies and the mode shape pattern for the model with a fixed shoulder and the model with shoulder motion. The natural frequencies of the model with a fixed shoulder are generally higher, suggesting that a fixed shoulder boundary condition stiffens the hand-arm system. For the model with fixed shoulder conditions, a mode around 13.0 Hz, which is closed to the frequency (12.5 Hz) of the maximum weight in the current ISO 5349-1 [9] frequency weighting, is not present. The model that permits shoulder motion exhibits a mode around 13.4 Hz (2nd mode), which is close to the frequency of the maximum weight in the current ISO weighting. Figure 4 shows that the first mode corresponds to a rigid rotation of the entire hand-arm system about the shoulder. This mode, which is common to both models, may be difficult to detect in the laboratory measurements of biodynamic responses for the extended-arm posture because the hand gripping the handle is constrained to move in the z_h-axis when uniaxial z_h-axis excitation is used, as shown in Figure 2. This mode, however, may be easily detected in measured biodynamic responses when the hand-arm is excited in the y_h-axis direction. Furthermore, the reported eigen analysis of different lumped-parameter models of the hand-arm derived from biodynamic responses showed that most of the models have their first natural frequencies in the 2.2−4.6 Hz range in the z_h-axis direction [6].

Table 3 and Figure 4 show that the 2nd mode (13.3 Hz), 8th mode (191.2 Hz) and 14th mode (456.2 Hz) are predominantly motion in the z_h-axis direction. The human hand-arm system may be subjected to repeated extension and compression, particularly at the joints, when excited at these modal frequencies and this may cause joint injury and musculoskeletal disorder. An interesting observation in Figure 4 is that the forearm and the upper-arm have higher natural frequencies (above 100 Hz). The study associated low natural frequencies (3.8, 12.7, 33.6 Hz) to the arms. The reported natural frequencies 112.5 Hz and 119.7 Hz are comparable with the 6th mode (107.5 Hz) and 7th mode (123.3 Hz), respectively in Table 3, which are associated with the wrist and palm. The present study clearly shows that the forearm and upper-arm also have high natural frequencies (above 100 Hz), which are not evident in the results of the lumped-parameter models probably due to limited degree-of-freedom (DOF). The maximum DOF in the reported lumped-parameter model was seven [7].

3.2 Comparisons of resonant frequencies of the models with those from experimental data

The resonant frequencies and damping ratios for the six subjects are derived from the stability diagrams of the OMA-ARMA analysis. An example of the frequency stability diagram is presented in Figure 3. The resonant frequencies are also obtained from the measured transmissibility responses, as explained in Section 2.2. Finally, the resonant frequencies of the FE models are obtained from harmonic responses at four different locations around the palm, wrist, elbow and shoulder designated as $X1-X4$ on Figure 1 in both the z_h- and y_h- axis.

Figure 5 illustrates the harmonic responses at different locations on the hand-arm model with shoulder motion in the z_h-axis. The responses are presented in both the linear (Fig. 5a) and logarithmic (Fig. 5b) scales to respectively highlight responses in low and high frequencies regions. The responses are considered on the muscles/tissues (e.g. Palm_m) and on the bone structures (e.g. Palm_b). Figure 5 shows that there is small difference between the bone structures and muscles/tissues responses below

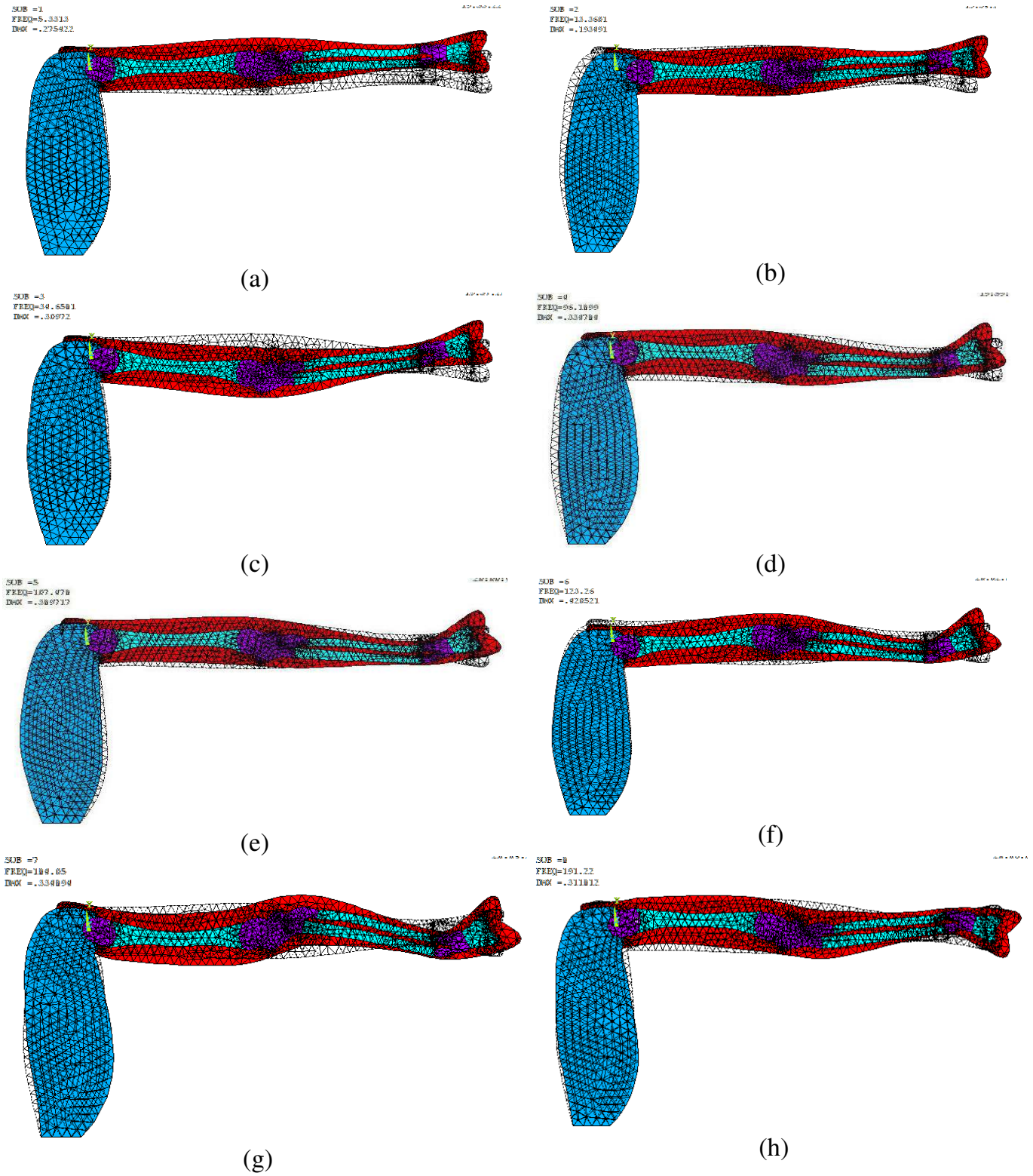

Fig. 4. Mode shapes of the hand-arm model that permits shoulder motion; (a) 1st mode at 5.3 Hz; (b) 2nd mode at 13.4 Hz; (c) 3rd mode at 34.7 Hz; (d) 4th mode at 96.2 Hz; (e) 5th mode at 107.5 Hz; (f) 6th mode at 123.3 Hz; (g) 7th mode at 184.1 Hz; and (g) 8th mode at 191.2 Hz.

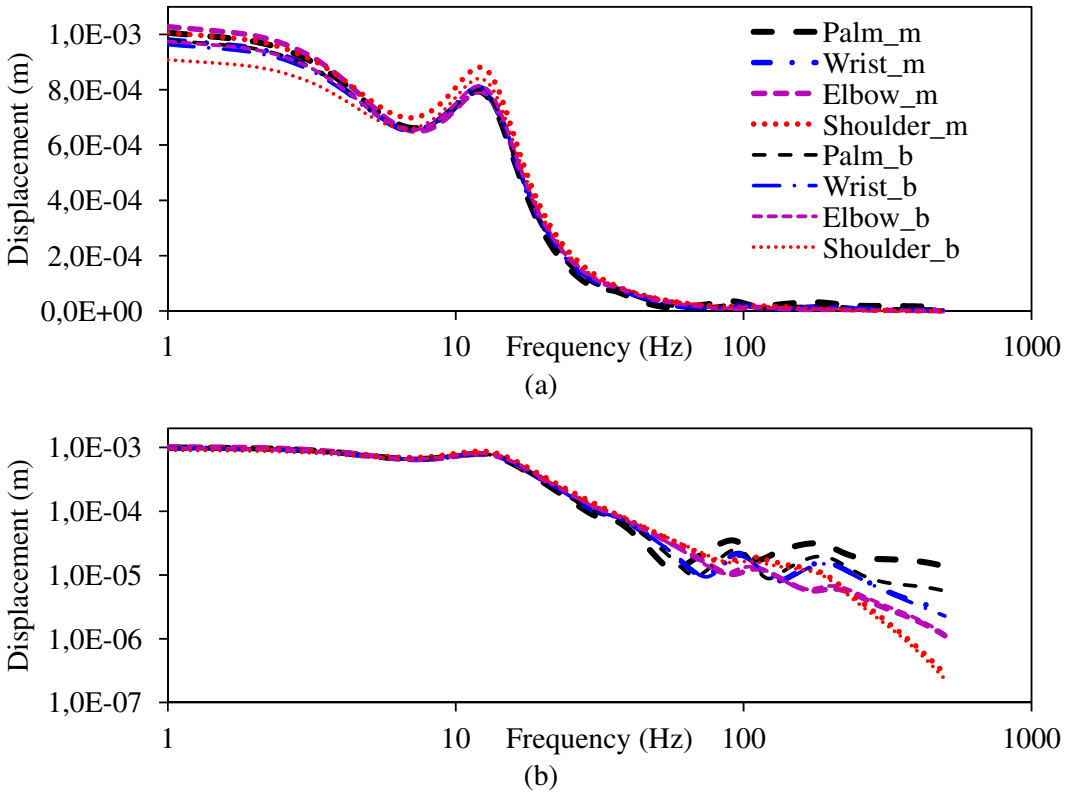

Fig. 5. Harmonic responses in the z_h-axis of bones and muscles for the FE model that permits shoulder motion around the palm ($X1$), wrist ($X2$), elbow ($X3$) and shoulder ($X4$); (a) linear scale of magnitude; (b) logarithmic scale of magnitude.

15 Hz for the shoulder responses and above 40 Hz for the palm responses; the responses at other locations are almost the same at all frequencies. Furthermore, Figure 5 shows small amplification of the elbow muscles response below 4 Hz and shoulder muscles response between 4 and 72 Hz. This trend is similar to that observed in the reported measured transmissibility responses, where amplification of the elbow and shoulder responses was reported below 15 Hz for the extended arm posture [11].

The resonant frequencies estimated from the measured transmissibility responses, and the harmonic responses of the FE models in the y_h- and z_h-axis are summarized in Table 4 for comparison. As observed in Table 3, the resonant frequencies derived from the FE model with a fixed shoulder are generally higher compared to the model that permits shoulder motion. A frequency about 12 Hz is conspicuous in the responses of the model that permits shoulder motion but not in the responses of the fixed shoulder model. Also, Figure 5b shows that the entire hand-arm system is excited in the z_h-axis around 12 Hz, and the animation of the 2nd mode (13.4 Hz) showed that the motion and deformation are predominantly in the z_h-axis, which results in continuous extension/compression of the joints and may cause the injury of the joints. This frequency (12 Hz) is close to the 12.5 Hz, which is the frequency with the maximum weight in the ISO 5349-1 [9] frequency weighting.

Some studies have suggested that the ISO 5349-1 [9] frequency weighting is good for assessing injury of the joints and musculoskeletal disorder in the arms of operators of low frequency power tools (e.g. sand rammers) who normally complain of pain in the arms, shoulder, neck and the head [17]. The 1st mode (about 3 Hz) is not very conspicuous in the measured transmissibility and harmonic responses of the FE models, and OMA-ARMA results. This may be attributed to the restriction of the excitation to z_h-axis, the hand-arm damping and the fact that the 1st mode is a rigid rotational motion about the shoulder. This frequency may be seen in the responses for excitation in the y_h-axis. Furthermore, the FE models did not show some resonant frequencies that are present in the measured transmissibility responses and the OMA-ARMA method (Tab. 5) probably due to the linearity assumptions in the FE modeling whereas the human hand-arm model is a highly non-linear system.

This suggests that the FE models need to be fine tuned since the mechanical properties of the human hand-arm system change with hand forces and posture. This may be achieved by slightly changing the reported mechanical properties of the hand-arm system until the FE models' responses are close to measured biodynamic responses. The results show that the FE model which permits shoulder motion is better than the model with a fixed shoulder since the former yields more frequencies that are comparable with frequencies derived from the measured experimental data. The following ranges of frequencies are common to the measured transmissibility responses, harmonic responses of the FE model that permits shoulder

Table 4. Resonant frequencies of the hand-arm system from the measured transmissibility responses and the harmonic responses of the finite element (FE) models.

Measured Transmissibility				FE model with fixed shoulder		FE model with shoulder motion	
z_h-axis		y_h-axis		z_h-axis	y_h-axis	z_h-axis	y_h-axis
Ranges (Hz)	Mean (Hz)	Ranges (Hz)	Mean (Hz)	(Hz)	(Hz)	(Hz)	(Hz)
Wrist					Wrist		
2.3−3.1	2.6	2.3−3.1	2.7				
7.0−7.8	7.4	4.7−9.4	7.1			12.0	12.0
10.4−14.8	11.9	18−25.6	21.2	36.0	37.0	36.0	33.0
21.1−23.4	22.5	30.4−39.8	36.6	127.0	127.0	96.0	104.0
42.2−44.5	43.7	59.4−78.9	69.3		304.0	191.0	245.0
93.8−127.3	106.3	114.8−129.7	123.2				400.0
143.0−179.7	165.1	200.0−230.0	215.0				
222.7−280.5	251.6	341.1−342.9	342.0		Elbow		
362.5−370.0	366.3	400.0−417.2	408.6		39.0	12.0	12.0
422.7−452.3	437.5			128.0	107.0	111.0	113.0
				270.0	202.0	209.0	185.0
Elbow					357.0		
2.3−3.9	2.8	2.3−3.1	2.9				
7.8−11.7	10.6	5.5−8.6	6.7		Shoulder		
15.6−18.8	16.6	10.2−11.7	10.8			12.0	12.0
21.9−25.9	23.5	14.1−18.8	16.0	41.0	41.0		33.0
28.1−36.7	32.4	31.3−35.9	34.2	128.0	135.0	103.0	97.0
61.7−71.1	66.4	54.5−81.3	65.3	330.0	329.0	178.0	179.0
91.4−112.5	103.0	91.4−105.0	100.1				
128.9−164.8	144.5	264.2−297.7	278.2		Palm		
241.2−248.4	244.8	362.5−369.5	366.0			12.0	12
				36	37	35.0	33.0
Shoulder				119	105	92.0	94.0
2.3−3.9	3.5	3.1−3.9	3.5		166	179.0	
6.3−7.0	6.8	6.3−9.4	7.7	335	348		
10.2−11.7	10.9	11.7−17.2	13.5				
14.1−17.2	15.7	21.1−28.9	24.8				
38.3−42.2	40.3	35.2−39.1	37.2				
50.0−54.7	52.4	48.4−53.9	50.2				
73.4−79.7	76.6	150.8−190.6	174.0				
91.4−103.9	97.7	239.1−241.5	240.3				
131.3−165.6	154.2						

motion and OMA-ARMA analysis: 11.9−12.3, 36.0−38.2, 97.0−97.8, 106.3−111.0, 174.0−177.9, 240.0−245.0 Hz.

4 Conclusions

Modal and harmonic analyses of a two-dimensional finite element (FE) model of the human hand-arm system are presented. Two boundary conditions were considered: the first is a fixed shoulder condition and the second is a model with the trunk to permit shoulder motion. The resonant frequencies were compared with those estimated from the measured experimental transmissibility responses and operational modal analysis using the autogressive moving average technique (OMA-ARMA). The results showed that the model that permits shoulder motion is a better model since the some of the derived resonant frequencies are closely related to the resonant frequencies determined from measured transmissibility responses and OMA-ARMA technique. Furthermore, the resonant frequency around 12 Hz was present in the responses of this model but not in the model with fixed shoulder. Animation of the second mode (13.4 Hz), corresponding to resonant frequency of about 12 Hz, for the model that permits shoulder motion showed that the entire hand-arm system was subjected to repeated extension/compression in the z_h-axis. This frequency (12 Hz) is close to the frequency of maximum weight (12.5 Hz) in the weighting recommended in the current International Standard Organization (ISO 5349-1, 2001) for the assessment of hand-arm vibration syndrome.

An improved finite element model of the human hand-arm system may be used to study stress/strain distribution in different substructures of the hand-arm system. This may give useful information about hand-arm injury mechanism, the understanding of which may assist in deriving appropriate frequency weightings for the assessment of different components of the hand-arm vibration syndrome.

Table 5. Comparisons of resonant frequencies of the human hand-arm system derived using different methods.

Measured transmissibility	FE model with shoulder motion	FE model with fixed shoulder	OMA-ARMA
2.6			
7.4			7.8
11.9	12.0		12.3
23.5			27.8
36.6	36.0	37.0	38.2
43.7			45.7
52.4			55.2
66.4			63.0
76.6			78.5
97.7	97.0		97.8
100.1	103.0		
106.3	111.0	107.0	109.1
144.5			145.7
154.2			
165.1		166.0	168.1
174.0	178.0		177.9
215.0			
240.3	245.0		240.0
251.6			255.5
342.0		348.0	341.8
437.5			439.2

Acknowledgements. This study is made possible by the Post-doctoral Fellowship awarded to the first author by the Natural Sciences and Engineering Council of Canada (NSERC). The authors therefore acknowledge the support of NSERC.

References

[1] M. Bovenzi, Exposure-response relationship in the hand–arm vibration syndrome: an overview of current epidemiology research, Int. Arch. Occup. Environ. Health 71 (1998) 509–519

[2] Y. Aldien, P. Marcotte, S. Rakheja, P.-É. Boileau, Influence of hand-arm posture on biodynamic response of the hand-arm exposed to z_h-axis vibration, IJIE 36 (2006) 45−59

[3] T. Nilsson, L. Burström, M. Hagberg, Risk assessment of vibration exposure and white fingers among platers, Int. Arch. Occup. Environ. Health 61 (1989) 473−481

[4] ISO 5349-1, Mechanical vibration and shock – Measurement and evaluation of human exposure to mechanical vibration, International Organization for Standardization, 2001

[5] M. Thomas, Y. Beauchamp, Development of a new frequency weighting filter for the assessment of grinder exposure to wrist-transmitted vibration, 22nd ICC&IE, 1997 Cairo, Egypt, Dec 20-22, 4p.

[6] S. Rakheja, J.Z. Wu, R.G. Dong, A.W. Schopper, A comparison of biodynamic models of the human hand-arm for applications to hand-held power tools, J. Sound Vib. 249 (2002) 55−82

[7] S.A. Adewusi, S. Rakheja, P. Marcotte, Biomechanical Models of the Human Hand-arm to Simulate Distributed Biodynamic Responses for Different Postures, Int. J. Ind. Ergon. 42 (2012) 249−260

[8] S. Adewusi, M. Thomas, H. Vu, Natural frequencies of the hand-arm system using finite element method, Proceedings of the 4th American Conference on Human Vibration, Hartford, Connecticut, USA, June 13–14, 2012, 17–18

[9] V.H. Vu, M. Thomas, A.A. Lakis, L. Marcouiller, Operational modal analysis by updating autoregressive model, Mech. Syst. Signal Process. 25 (2011) 1028−1044

[10] J.Z. Wu, R.G. Dong, S. Rakheja, A.W. Schopper, Simulation of mechanical responses of fingertip to dynamic loading, Med. Eng. Phys. 24 (2002) 253–264

[11] S.A. Adewusi, S. Rakheja, P. Marcotte, J. Boutin, Vibration transmissibility characteristics of the human hand-arm system under different postures, hand forces and excitation levels, J. Sound Vib. 329 (2010) 2953−2971

[12] D.D. Reynolds, E.N. Angevine, Hand-arm vibration. Part II: vibration transmission characteristics of the hand and arm, J. Sound Vib. 51 (1977) 255−265

[13] H. Sakakibara, T. Kondo, M. Miyao, S. Yamada, T. Nakagawa, F. Kobayashi, Y. Ono, Transmission of hand-arm vibration to the head, Scand. J. Work Environ Health 12 (1986) 359−361

[14] G.J. Loren, R.L. Lieber, Tendon biomechanical properties enhance wrist muscle specialization, J. Biomechanics 128 (1995) 791−799

[15] C.N. Maganaris, J.P. Paul, In vivo human tendon mechanical properties, J. Physiol. 521 (1999) 307−313

[16] D.C. Wirtz, T. Schiffers, T. Pandorf, K. Radermacher, D. Weichert, R. Forst, Critical evaluation of known bone material properties to realize anisotropic FE simulation of the proximal femur, J. Biomech. 33 (2000) 1325−1330

[17] J.H. Dong, R.G. Dong, S. Rakheja, D.E. Welcome, T.W. McDowell, J.Z. Wu, A method for analyzing absorbed power distribution in the hand and arm substructures when operating vibration tools, J. Sound Vibr. 311 (2008) 1286−1304